Power Allocation Scheme for OCDMA NG-PON With Proportional–Integral–Derivative Algorithms

Thiago A. Bruza Alves, Fábio R. Durand, Bruno A. Angélico, and Taufik Abrão

***Abstract*—Distributed power control algorithms (DPCAs) based on the Foschini/Miljanic (FM) and Verhulst (V) models and a proportional–integral–derivative (PID) algorithm have been investigated in this work for next-generation passive optical networks (NG-PONs). The DPCAs of FM and V that are represented by the classical control theory as an integral control present limitations in the accuracy of signal-to-noise-plus-interference ratio (SNIR) estimates in weak-signal environments. Furthermore, in this work the development of DPCA-PID-FM and DPCA-PID-V based on PID schemes originated as DPCA-FM and DPCA-V, respectively, has been conducted to overcome the SNIR estimation limitation. The main results have shown that DPCA-FM reaches convergence with a lower number of iterations than DPCA-V for situations of a good SNIR. However, under weak-signal scenarios, DPCA-V exhibits a smaller discrepancy from the optimum power vector solution and better convergence than DPCA-FM. Also, the proportional and differential actions taken in DPCA-V to originate DPCA-PID-V do not present a noticeable impact on the tendency and the velocity of the convergence compared with DPCA-V. On the other hand, DPCA-PID-FM changes the trend in convergence from DPCA-FM. Finally, the increase in channel error estimation causes an error of convergence for all DPCAs studied in this work. The main advantage of DPCAs based on PID is the possibility of utilizing adaptive tuning procedures to tune the PID gains.**

***Index Terms*—Distributed power control algorithms; Optical networks; Proportional–integrative–derivative.**

I. Introduction

The passive optical network (PON) is the leading cost-effective networking technology for fiber-to-the-home broadband access and backhauling for mobile broadband networks [1–3]. The point-to-multipoint architecture is composed of an optical line terminal (OLT) at the service operator side and optical network units (ONUs) at the client side [2]. The present PON standards commercially available are 10 Gbit capable PON and 10 Gbit Ethernet PON networks, which are categorized as next-generation PON stage 1 (NG-PON1) [2]. These networks are based on time-division multiplexing (TDM) technology with a 10 Gbps transmission rate [4]. The natural evolution of NG-PON1 to NG-PON2 (stage 2) aims to enlarge the coverage area while increasing the transmission rate and expanding the number of ONUs [3,4]. Furthermore, NG-PON2 requirements include at least 40 Gbps capacity in downstream and at least 10 Gbps capacity in upstream [4]. The standardization and industrial groups have appointed the hybrid time- and wavelength-division multiplexing as a potential solution to meeting the NG-PON2 requirements [4]. However, considering the technological limitations featured by the TDM technique and the availability of the wavelength-division multiplexing (WDM) spectral range, the disruptive NG-PON3 (stage 3) technology will require the accommodation of ever-increasing traffic.

The development of the technologies beyond NG-PON2, such as NG-PON3, will be based on the use of technologies such as WDM, orthogonal frequency-division multiplexing, and optical code division multiple access (OCDMA), as well as an advanced modulation format where these technologies can be used in a single way or together [1–3]. In this context, the evolution to NG-PON3 presents some challenges such as extension of the optical power budget, fiber impairment mitigation (including linear and nonlinear effects), and dynamic resource allocation [5,6]. In addition, it is fundamental that we investigate and improve the energy efficiency and spectral efficiency of the entire network, considering the highly bursty traffic behavior, the increasing number of ONUs, and the expansion tendency of these networks [7].

OCDMA is a potential technology for NG-PON, considering its characteristics such as asynchronous operation, high network flexibility, protocol transparency, simplified network control, and potentially enhanced security [5,6,8]. In OCDMA networks, each different code defines an ONU, and different code ONUs can share a common channel. The interference among different codes is called multiple access interference (MAI) and could be a limitation in the simultaneous utilization of the channel by code users [6,9]. An OCDMA approach based on a single multiport encoder/decoder (E/D) at the OLT and superstructured fiber Bragg grating (SSFBG) E/D at the ONUs was developed as a candidate to go beyond NG-PON2 [10]. This

Manuscript received March 28, 2016; revised July 13, 2016; accepted July 14, 2016; published August 8, 2016 (Doc. ID 262046).

T. A. Bruza Alves and T. Abrão (e-mail: taufik@uel.br) are with the State University of Londrina, Electrical Engineering Department, Paraná 86057-970, Brazil.

F. R. Durand is with the Federal University of Technology—Paraná at Cornélio Procópio, Cornélio Procópio, Paraná 86300-000, Brazil.

B. A. Angelico is with the University of São Paulo, São Paulo, São Paulo 05508-900, Brazil.

http://dx.doi.org/10.1364/JOCN.8.000645

scheme could reach a bidirectional transmission rate of 40 Gbps; the use of a multiport E/D can aggregate the OLT, whereas the optical E/D processing a single optical code at each ONU is a low-cost device with a small footprint. This approach can improve the cost-effectiveness and the system flexibility regarding the demand of ONUs when combined with the WDM technique. Hence, considering the potential of the related OCDMA scheme, this technology is considered in the present work, namely, 40G-OCDMA-PON.

In PONs, one fundamental resource is the transmitted power of the ONUs; moreover, the dynamic optimization of the transmitted power improves the network flexibility, capacity, and energy efficiency [11,12]. There are different algorithms for dynamic optimization of the transmitted power applying different principles, such as game theory, local search, and heuristic-based algorithms, namely, simulated annealing, genetic algorithms, particle swarm optimization, and ant colony optimization [8]. The main features of such algorithms include (a) the power transmission adjustment, (b) the multiple bit rate capability, and (c) the control of the active ONUs, with the goal of obtaining the maximum aggregate throughput of the PONs [12–14]. However, the computational complexity and unfairness in such schemes are aspects that need to be improved [8,9]. In this context, the analytical iterative distributed power control algorithms (DPCAs) proposed initially for wireless networks, such as the Foschini and Miljanic algorithm (DPCA-FM) [15] and one based on the Verhulst model (DPCA-V) [16], represent potential solutions for resource allocation in PONs with a lower computational complexity. DPCA-FM is based on the linear update scheme that results from the approach to solving an ordinary differential equation related to the power control of the transmitted power. On the other hand, DPCA-V is based on the Verhulst model, which attempts to describe the development over time of the number of individuals of some biological species. The main aspects considered in the model are the limits of the physical space and food, which are related to the delimitation of the population growth [17]. Although these DPCAs were proposed for a wireless network environment, both have been adapted to optical network scenario [11,17].

Interestingly, DPCA-FM and DPCA-V could be represented by the classical control theory as an integral (I) control with some differences in the error function [18]. In this sense, with the objective of obtaining a more accurate control capability, the proportional (P) and derivative (D) terms could be added to DPCA-FM and DPCA-V, aiming to obtain power allocation schemes based on a proportional–integral–derivative (PID) algorithm. The PID approach has been previously studied for power control in a wireless network environment based on the DPCA-FM power control algorithm [19]. This approach can overcome the limitation of DPCAs based on type I controllers due to the accuracy of signal-to-noise-plus-interference ratio (SNIR) estimates in weak-signal environments [20].

In this sense, the main contribution of this work consists of the investigation and characterization of PID DPCA-FM- and DPCA-V-based power control algorithms directly applicable to the next 40G-OCDMA-PONs. Aspects of DPCA-PID-FM and DPCA-PID-V based on PID schemes, together with DPCA-FM and DPCA-V, are extensively analyzed and compared in this contribution. For the PID distributed power control approach, one can point out its benefits, comparing performance, complexity, and fairness with other optimization methods that utilize matrix inversion, numerical procedures, and other heuristic schemes. In this work, important aspects of convergence, performance, complexity, and channel estimation will be investigated, aiming to evaluate the effectiveness of the proposed DPCAs in specific NG-PON environments.

The rest of this paper is organized in the following manner. In Section II the optical network architecture is presented, while in Section III the power control algorithms for NG-PON are discussed. Section IV illustrates the methodology utilized to evaluate the DPCAs applicable to NG-PONs. Afterward, numerical results are discussed in Section V. Finally, the main conclusions are offered in Section VI.

II. 40G-OCDMA-PON Architecture

The NG-PON based on a 40GE-OCDMA-PON architecture is shown in Fig. 1. In this architecture the multiport E/D at the OLT is based on multiport arrayed waveguide gratings (AWGs) for generating and recognizing multiple time-spreading optical codes in a single device simultaneously [6]. The E/Ds at the ONUs are based on a SSFBG, which has features such as polarization-independent performance, low insertion losses, independence of the code length, and good connectivity with the optical fiber [10]. The code generated in the OLT and ONUs is categorized as coherent code phase-shift keying (PSK), in which the code information is embedded for the phase [5].

In the multiport E/D at the OLT, the mechanism for building a set of optical codes can be described based on an AWG with N inputs/outputs in the time domain. If a short light pulse is driven into one of the device inputs, N copies of the pulse will be generated by the input slab coupler, with phases given by the Rowland circle configuration [21]. The optical pulses travel different paths in the grating, and the output slab coupler recombines the pulses to build N codes at the device outputs. Each PSK-modulated code is composed of N optical chips, and the differential path delay in the grating is chosen to be larger than the input pulse width, so that the chips in the optical code do not overlap. Thus, each PSK code is obtained through a combination of N light pulses with different phases. The chip period (T_C), which represents the time interval between two consecutive pulses in each optical code, is defined as $T_C = n_s \Delta L/c$, where n_s is the waveguide refraction rate and c is the speed of light [11]. The chip interval is equal to the inverse of the free spectral range, and the number of generated codes (cardinality) depends on the combination of pulses at the device input. Moreover, by employing a combination of $N/2$, we can obtain a cardinality given by the binomial $\binom{N}{N/2}$, where N is the code length.

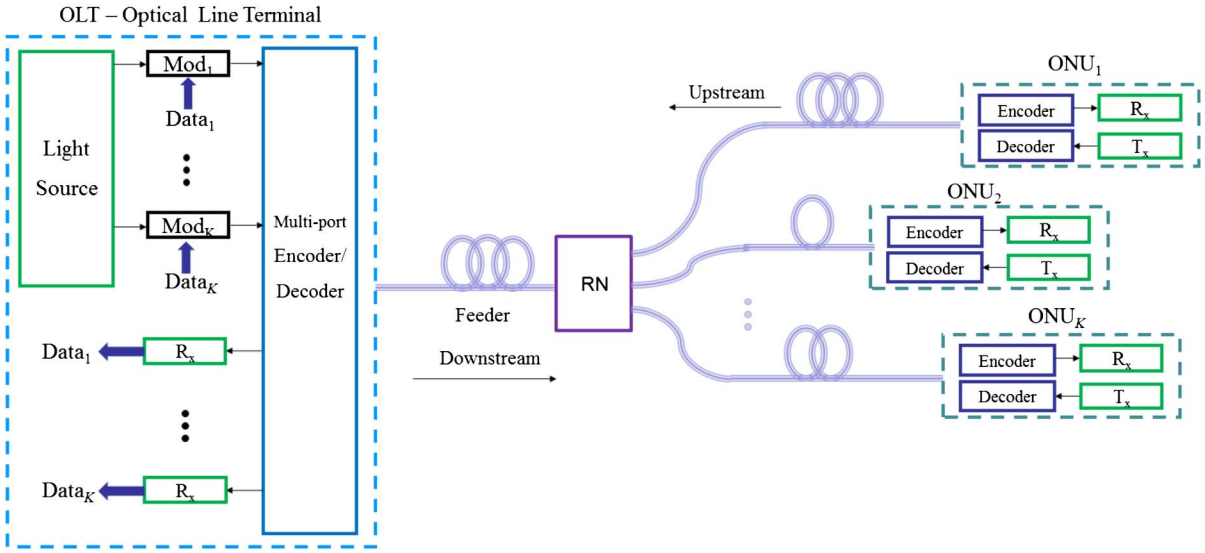

Fig. 1. 40G-OCDMA-PON network architecture with optical line terminal (OLT), optical network unit (ONU), and remote node (RN).

The maximum cross-correlation of these code sets is given by $(N-1)^2$, and the autocorrelation peak is given by N^2 [20]. However, for the case of the OCDMA system based on an AWG E/D, the power contrast ratio (PCR) between the autocorrelation and the cross-correlation depends on the AWG E/D architecture [6,21,22,23]. The optimized AWG E/D architectures can provide a high level of PCR, such as the multiport E/D with more than 35 dB for the AWG with a 128×128 port [24].

In the SSFBG at the ONU, an optical code sequence is obtained by reflecting back optical chip pulses from each fiber Bragg grating (FBG) chip. A SSFBG is defined as a special class of FBG in which many short grating segments along the fiber axis configure the total grating. In the PSK code, assignment of the multilevel code information for each chip can reduce the influence of MAI noise; the correlation property of this code is superior to other coherent code sequences [11]. To generate time-spreading PSK code in the SSFBG, the number of FBG chips and the phase-shift level for desired code sequences must be adjusted. This SSFBG also acts as the decoder, resulting in either the autocorrelation or cross-correlation waveform according to its FBG chip arrangement [11,25].

III. Power Control Algorithms

The main problem in optical resource management is the power allocation and the associated energy efficiency network optimization. In this section the power allocation problem for NG-PONs is reformulated under the PID perspective.

A. Power Allocation Problem

The allocation of the transmitted power or the optical power control in the ONUs under PON scenarios can be characterized as an optimization problem. The performance metric of the maximum acceptable bit error rate (BER) in the OLT is associated with the carrier-to-interference ratio (CIR) at the particular decoder [17]. The optical power control problem consists of determining the optical power vector $\mathbf{p}$ that minimizes the cost function [9,11], $J(\mathbf{p}) = \mathbf{1}^T\mathbf{p} = \sum_{i=1}^{K} p_i$, subject to the constraints [26,27]

$$\Gamma_i = \frac{G_{ii}p_i(n-n_{ii})}{\sum_{j=1,j\neq i}^{K} G_{ij}p_j(n-n_{ij}) + \sigma^2} \geq \Gamma_i^* \quad p_{\min} \leq p_i \leq p_{\min}, \tag{1}$$

where Γ_i is the CIR, $\mathbf{p} = [p_1, p_2, \ldots, p_K]^T$ is the K-dimensional column vector of the transmitted optical power, and $\mathbf{1}^T = [1, \ldots, 1]$. Γ^* is the minimum CIR related to a satisfactory quality of service (QoS), G_{ij} represents the connections of transmitter–receiver pairs, σ^2 is the total power of receiving noise explicitly described in Subsection IV.A, p_i is the transmitted power for the ith ONU, and p_j is the transmitted power for the interfering user's ONUs. Note that n_{ii} represents the time delay on the updating of the transmitted power perceived at the power control algorithm between the ith transmitting node and ith receiving node, while n_{ij} represents the time delay on the power interfering user's signal j perceived by the power control algorithm of the interest user's i. Hence, this time delay is calculated for each ONU based on link length (propagation delay), processing time, and the updating of the power control algorithm [26,27].

The CIR illustrated in Eq. (1) can be presented as $[\mathbf{I} - \Gamma^*\mathbf{H}]\mathbf{p} \geq \mathbf{u}$ based on matrix notation, where $\mathbf{I}$ is the identity matrix and $\mathbf{H}$ is the normalized interference matrix, whose elements can be represented by $H_{ij} = G_{ij}/G_{ii}$ for $i \neq j$ and zero otherwise [8]. In addition, the scaled version of the noise power is given by $u_i = \Gamma^*\sigma^2/G_{ii}$. To obtain the power vector solution, the inequality above can be substituted by the equality, and the optimized power vector

solution is obtained by the matrix inversion [9], i.e., $\mathbf{p}^* = [\mathbf{I} - \Gamma^*\mathbf{H}]^{-1}\mathbf{u}$. Hence, this matrix operation is characterized by a high computational complexity; in addition, the matrix inversion represents a case with centralized power control, for which a central node should be supplied with information about physical network aspects, such as the fiber length between OLTs and ONUs, amplifier position, and regular updates for the traffic dynamics [17]. These observations justify the need for distributed SNIR optimization algorithms, which should present suitable convergence properties for general network configurations [11,13].

B. Distributed Power Control Algorithms

The main feature of the DPCAs is their ability to be executed in each ONU based on the accessibility of local information such as the SNIR level and the transmitted power in the ONUs [14]. Therefore, these algorithms are related to only local parameters, allowing just the power control to work in a distributed manner [8].

DPCA-FM is based on the progress of an iterative process for the vector $\mathbf{p}$ evolution aiming to achieve the optimum value $\mathbf{p}^*$, based on the SNIR (γ) and the target SNIR (γ_i^*). The iterative process results in an optimum solution for the power allocation problem given by [15]

$$p_i[n] = p_i[n-1] - \alpha\left(1 - \frac{\gamma^*}{\gamma[n]}\right)p_i[n-1], \tag{2}$$

where n is the number of iterations and α is the numerical integration step that allows power convergence in the range of $0 < \alpha < 1$ [17]. On the other hand, DCPA-V, in terms of the power update for each ONU in the PON, can be described by [16]

$$p_i[n] = p_i[n-1] + \alpha\left(1 - \frac{\gamma[n]}{\gamma^*}\right)p_i[n-1]. \tag{3}$$

For both DCPA-FM and DPCA-V, α is the numerical integration step for solving ordinary differential equations associated with the power control algorithms. This factor is related to the velocity of the convergence and quality of the solution, and is limited by $0 < \alpha < 1$. For values near 0, convergence is slow; however, the quality of the solutions is adequate. On the other hand, for values near 1, the convergence is fast; however, the quality of the solutions in certain scenarios can be remarkably affected [17,28]. The quality of the solution (after convergence), in terms of the normalized mean squared error (NMSE), is related to the optimal solution $\mathbf{p}^*$ and calculated as

$$\mathrm{NMSE}[n] = E\left[\frac{\|\mathbf{p}[n] - \mathbf{p}^*\|^2}{\|\mathbf{p}^*\|^2}\right], \tag{4}$$

where $\|\cdot\|$ denotes the square Euclidian distance to the origin and $E[\cdot]$ is the expectation operator. Hence, a simple indicator of the quality of the solution achieved by DPCAs is how close to the optimum solution $\mathbf{p}[n]$ is at the nth iteration.

C. PID Power Control Algorithm

In the PID control, the principle of the I action is to guarantee that the process output agrees with the reference value in a steady state, and it is associated with the accumulation of previous errors. In addition, the P term is responsible for overall control that is proportional to the error performed and conducts the present error. The D term is responsible for improving the stability and performs a prediction of the future errors [14]. Furthermore, the original DPCA-FM and DPCA-V only take into consideration the I term of the PID power control description.

Let's consider the DPCA-FM algorithm in Eq. (2). By defining

$$e_i[n] = \left[1 - \frac{\gamma^*}{\gamma[n]}\right]p_i[n-1], \tag{5}$$

the difference equation becomes

$$p_i[n] = p_i[n-1] - \alpha e_i[n]. \tag{6}$$

In the z domain,

$$P_i(z) = \frac{-\alpha}{1 - z^{-1}}E_i(z), \tag{7}$$

which is essentially an integral controller. For DPCA-V, by defining

$$e_i[n] = \left[1 + \frac{\gamma[n]}{\gamma^*}\right]p_i[n-1], \tag{8}$$

the difference equation becomes

$$p_i[n] = p_i[n-1] + \alpha e_i[n]. \tag{9}$$

In the z domain,

$$P_i(z) = \frac{\alpha}{1 - z^{-1}}E_i(z), \tag{10}$$

which is also an integral controller.

The DPCA-PIDs based on the related DPCA-FM and DPCA-V, named herein DPCA-PID-FM and DPCA-PID-V, respectively, could be obtained by adding the proportional and derivative terms as well. For DPCA-PID-V, the transfer function for the ith ONU can be given by

$$\frac{P_i(z)}{E_i(z)} = -\beta - \frac{\alpha}{1 - z^{-1}} - \theta(1 - z^{-1}), \tag{11}$$

where β, α, and θ are the proportional, integral, and derivative gain, respectively. The DPCA-PID-FM difference equation is written as

$$\begin{aligned} p_i[n] = p_i[n-1] &- \beta(e_i[n] - e_i[n-1]) - \alpha e_i[n] \\ &- \theta(e_i[n] - 2e_i[n-1] + e_i[n-2]). \end{aligned} \tag{12}$$

For DPCA-PID-V, the difference equation can be given by

$$p_i[n] = p_i[n-1] + \beta(e_i[n] - e_i[n-1]) + \alpha e_i[n] + \theta(e_i[n] - 2e_i[n-1] + e_i[n-2]). \quad (13)$$

IV. PON Network Performance Analysis

In this section, the paramount figures of merit in optical network characterization are revisited, including signal-to-noise interference, the impact of error estimation on the performance, and a measure of computational complexity.

A. Signal-to-Noise Plus Interference

In order to achieve a specific QoS, that is related to a maximum BER tolerated by the OLT, based on an upstream of K ONUs, the SNIR at the required decoder input can be defined as [12,18,19]

$$\gamma_i = \frac{N^2}{\rho^2}\Gamma_i, \quad (14)$$

where ρ is the Hamming average variance of the cross-correlation amplitude [25]. G_{ij} represents the $i-j$ connection of transmitter–receiver pairs in linear units:

$$G_{ij} = 2a_C L_C \exp(-\alpha_f d_{ij}) \quad (15)$$

where α_f is the fiber attenuation (km^{-1}), a_c represents the E/D attenuation (linear units), and L_c is the total internal loss in the optical path. There is the establishment of the virtual path between the transmitting ONU and receiving OLT based on the code and the total link length, which is represented by [9]

$$d_{ij} = d_i^{tx} + d_j^{rx}, \quad (16)$$

where d_i^{tx} is the link length from the transmitting ONU to the remote node and d_j^{rx} is the link length from the remote node to the OLT [9].

The receiver noise power σ^2 in Eqs. (1) and (14) consists of three terms: the thermal noise, shot noise, and amplified spontaneous emission (ASE) preamplifier noise. However, the ASE in the optical preamplifier is very representative (in addition to the MAI) when confronted with the thermal and shot noise at the receiver side [11,12]. Accordingly, the receiver noise power is given by [11]

$$\sigma^2 = 2n_{\mathrm{SP}}hf(G_{\mathrm{amp}} - 1)B_0, \quad (17)$$

where the constant value 2 is due to the two polarization modes presented in a single-mode fiber, n_{SP} is the spontaneous emission factor, typically in the range $n_{\mathrm{SP}} \in [2;5]$, h is Planck's constant, f is the carrier frequency, G_{amp} is the amplifier gain, and B_0 the optical bandwidth [9]. If more than one amplifier is needed in the power budget [9], the recursive model for computation of the ASE at cascaded amplified spans will be utilized [13].

B. Channel Error Estimation

In the DPCA procedure, the channel error estimation is based on the uncertainty in the SNIR estimation in each update. The uncertainties occur in the SNIR estimation process, which is related to the optical channel error estimation in the receiver node. Moreover, the estimation process could include combinations of analytical models and/or interpolations of measurements and simulations [29]. The SNIR parameter at each node is imperfectly estimated; some parameters of the received sample distribution depend not only on the transmitted pulse shape, filter types, and bandwidths but also on the channel impairments, mainly group velocity dispersion and ASE, and on the noise power spectral density [29]. Therefore, the values obtained from these estimations present a random error characteristic represented herein by the random variable ϵ. On the other hand, this random variable depends on what monitoring information is available in the network to perform the estimation. In this context, the random error is added to each channel (G_{ii}), resulting in the channel error estimation, and consequently this error is incorporated into the calculated SNIR during the iterative process. The ratio of the estimated channel matrix ($\hat{\mathbf{G}}$), and the real channel matrix ($\mathbf{G}$) values is given by $(1+\epsilon)$ within $\epsilon \in [-\delta;\delta]$. Therefore, the estimated channel matrix $\hat{\mathbf{G}}$, at each iteration, is represented by [17]

$$\hat{\mathbf{G}} = (1+\epsilon)\mathbf{G}, \qquad \forall\, i \quad \text{and} \quad \epsilon \in [-\delta;\delta]. \quad (18)$$

Furthermore, in this work, the error in the channel estimation is considered a random variable with a uniform distribution in the range $\delta \sim U[0;1]$.

C. Delay Effect Compensation

In PONs the signal propagation delay cannot be ignored, because there is a round-trip propagation bigger than the propagation delay of wireless CDMA-based networks [26,27]. If the processing time (including coding, decoding, and waiting for channel availability) is considered in addition to the signal propagation delay, the time delay can be tens of milliseconds [28]. However, unlike in wireless networks, in PONs the information about the round-trip delay is known [27,28,30]. The total round-trip delay between the ith transmitting node and ith receiving node is given by $n_{ii}^{RT} = n_f + n_b + 1$, where n_f and n_b represent the forward and backward delays in the feedback system, respectively [28]. In addition, an extra delay period could be added due to the processing time. In this context, where the round-trip delay is known, the traditional Smith predictor method can be utilized with the power control algorithms to compensate the total round-trip delay [31–33].

D. Complexity Analysis

The computational complexity of the DPCAs is evaluated based on the execution time, which quantifies the

amount of time taken by an algorithm to run until convergence (or at least until the ith iteration), as a function of the mathematical number of operations and number of ONUs. In the DPCAs studied, the computational complexity is related to the number of executed operations, including sums and multiplications, as well as the number of iterations necessary for the full convergence of the algorithm. The computational complexity of the DPCAs could be found in a same way as that discussed in [34], and it has been found that the DPCAs' polynomial complexity is dominated by the operations in Eq. (1). Thus, the computational complexity of DPCA-FM and DPCA-V is of the order $\mathcal{O}(K^2)$, where K is the number of ONUs per wavelength. Moreover, DPCA-PID-FM and DPCA-PID-V do not increase the computational complexity order when compared with DPCA-FM and DPCA-V, since no further dominant computational complexity term has been introduced.

In order to perform a more representative comparison, the time complexity of the centralized power control algorithm (performed by the matrix inversion procedure) is also evaluated. Thus, considering that centralized power control is based on matrix inversion, the time complexity in the best case is given by $\mathcal{O}(K^2 \cdot \log K)$ [34].

V. Numerical Results

In this section relevant aspects of convergence, performance, and the effects of channel estimation are investigated. An individual transmission rate equal to 40 Gbps has been assumed for each ONU, related to technologies for network scalability described in [5,6,10]. Table I summarizes the main system parameters deployed in the numerical simulation trials. In the optical network scenario, the link length from the OLTs to the remote node is 40 km. Moreover, the link lengths from the remote node to the ONUs are uniformly distributed over a distance with a radius between 2 and 50 km. Hence, the range of the total link lengths is [42; 90] km. In DPCA-FM and DPCA-V the parameter α is equal to 0.5, with the objective to obtain a suitable trade-off between the convergence speed and the quality of the solution. On the other hand, in DPCA-PID-FM and DPCA-PID-V the gains of the PID should be tuned aiming to attain full convergence [35]. In [19] a general power control PID-based algorithm is suggested. It considers multiple candidate PID gains, and, depending on the channel conditions, an algorithm selects the best PID gains (P, I, and D terms), resulting in a switching-based controller [19]. In the present work, only a set of gains is considered, whose parameters are $\beta = 0.5$, $\alpha = 0.2$, and $\theta = 0.2$. These values were obtained empirically.

TABLE I
System Parameters

Variable	Value
α_f: Fiber loss coefficient	0.2 dB/km
d_{ij}: Link length	[42: 90] km
h: Planck constant	6.63×10^{-34} J/Hz
f: Light frequency	193.1 THz
B_o: Optical bandwidth	100 GHz
n_{sp}: Spontaneous emission factor	2
G_{amp}: Erbium-doped fiber amplifier gain	20 dB
R_c: Chip rate	320 Gchips
N: Code length	64
R_i: Individual bit rate	40 Gbps
L_{AWG}: Losses of AWG	16 dB
L_{Bragg}: Losses of Bragg	6.7 dB
P_{min}: Minimum transmitted power	−100 dBm
P_{max}: Maximum transmitted power	20 dBm
γ_i^*: Target SNIR	20 dB

Without loss of generality, in the initial results the time delay has been considered compensated, as described in Subsection IV.C. In these results, the main idea was to evaluate the performance of DPCA-FM and DPCA-V using SNIR estimates in weak-signal environments. In addition, the performance evaluation of DPCA-PID-FM and DPCA-PID-V will be conducted under the same SNIR conditions. After that, the effects of delay in DPCA-PID-FM and DPCA-PID-V will be analyzed.

In order to evaluate the DPCA-FM and the DPCA-V convergence performance and quality of the solution, Fig. 2 depicts the power allocation evolution per ONU for the number of iterations considering (a) DPCA-FM and (b) DPCA-V for 32 ONUs. This PON, with the number of ONUs equal to 32, represents an optical scenario with SNIR estimates in strong-signal environments. The horizontal dashed lines represent the centralized power allocation per ONU obtained via the matrix inversion procedure. Accordingly, the matrix inversion procedure has been utilized to validate the convergence of our numerical results.

It can be observed in Fig. 2 that the power allocation per ONU reaches convergence for both conventional iterative power allocation schemes, i.e., DPCA-FM and DPCA-V. However, DPCA-FM reaches convergence with a lower number of iterations than DPCA-V. When Figs. 2(a) and 2(b) are compared, there is a difference of approximately 50 iterations for the convergence of DPCA-V compared to DPCA-FM. This tendency is related to Eqs. (2) and (3)

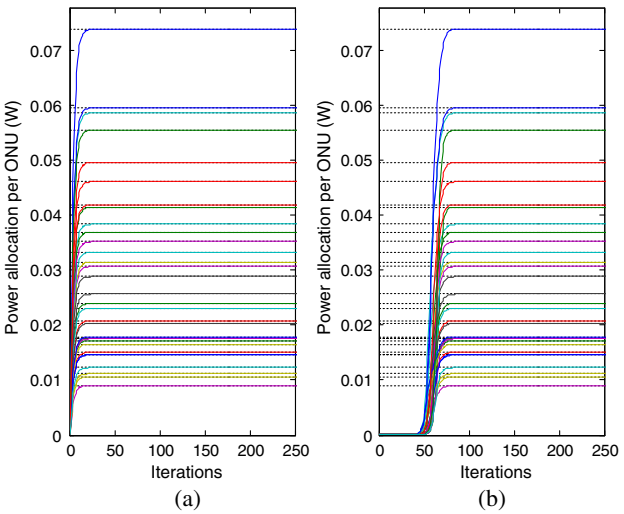

Fig. 2. PON-OCDMA with 32 ONUs. Power allocation per ONU for (a) DPCA-FM and (b) DPCA-V.

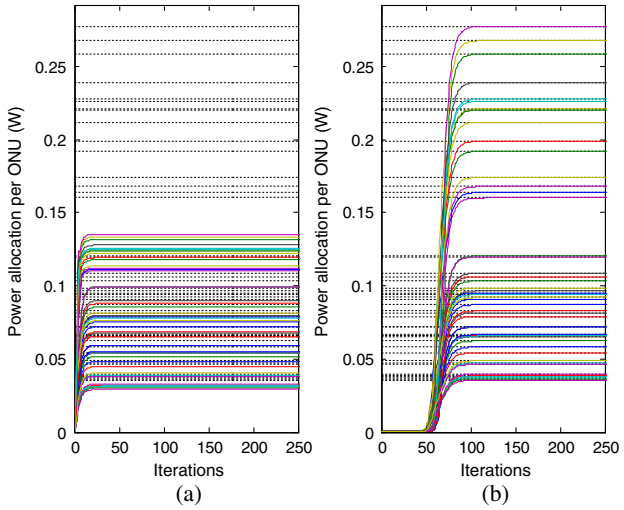

Fig. 3. PON-OCDMA with 48 ONUs. Power allocation per ONU for (a) DPCA-FM and (b) DPCA-V.

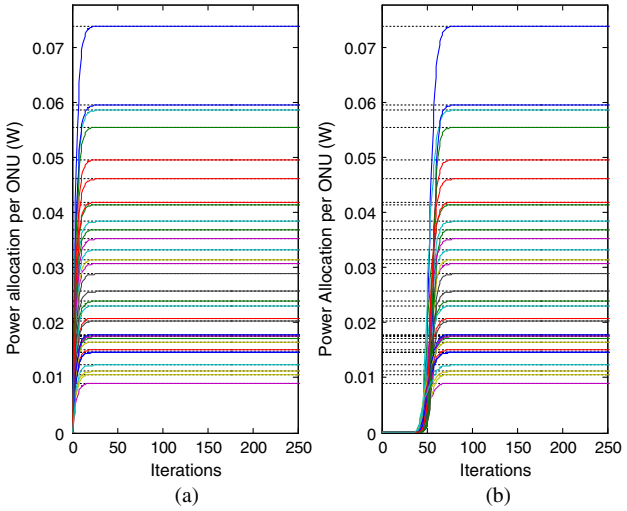

Fig. 4. PON-OCDMA with 32 ONUs. Power allocation per ONU for (a) DPCA-PID-FM and (b) DPCA-PID-V.

based on the second term of the equations to be subtracted or added in DPCA-FM and DPCA-V, respectively. In addition, the slow convergence of the DPCAs is related to the adoption of low values of α; this choice aims to obtain a final solution (after convergence) without degradation [17,28].

Figure 3 shows the power allocation evolution per ONU for the number of iterations considering DPCA-FM [Fig. 3(a)] and DPCA-V [Fig. 3(b)] for 48 ONUs. This scenario, based on the increase in the number of PONs, has been conducted to evaluate the SNIR estimates in weak-signal environments.

It can be observed in Fig. 3 that the power allocation per ONU does not reach full convergence for DPCA-FM; only DPCA-V reaches full convergence, but with the number of iterations for 48 ONUs being greater than the number of iterations for the case with 32 ONUs. The problem of the DPCA-FM convergence is related to the formalism in Eq. (3). In this formalism, the SNIR (γ) is in the denominator, like the representation $\phi = \kappa\gamma^{-1}$; hence, this function presents a differential increment given by $d\phi = -\kappa\gamma^{-2}\, d\gamma$. In this context, the value of ϕ variation for small γ deviations is related to the actual value of γ. Accordingly, in DPCA-V the SNIR (γ) is in the numerator, i.e., $\phi = \kappa\gamma$. Hence, the value of ϕ variation presents a differential increment of $d\phi = -\kappa d\gamma$, which is independent of the actual value of γ. This particularity of DPCA-V became the algorithm's sensitivity independent of the SNIR real value. As a result, in estimated weak-signal scenarios, DPCA-V exhibits a smaller discrepancy from the optimum power vector solution and better convergence than DPCA-FM [17]. In addition, it is worth noting that DPCA-FM does not reach its target SNIR because the maximum transmitted power is reached. Therefore, considering the integration action of this algorithm, the transmitted power will be constantly increased until the regulation error in Eq. (2) is zero. However, the increase in this value will result in the appearance of nonlinear effects in the optical fiber [17]. The nonlinear effects will degrade the optical signal and damage the optical network performance. DPCA-FM does not reach its target SNIR for 48 ONUs, as illustrated in Fig. 3, because the maximum transmitted power is reached and an increase in this value will result in the appearance of nonlinear effects in the optical fiber.

In order to evaluate the DPCA-PID-FM and the DPCA-PID-V performance related to convergence and quality of the solution, Fig. 4 shows the power allocation evolution per ONU for the number of iterations considering DPCA-PID-FM [Fig. 4(a)] and DPCA-PID-V [Fig. 4(b)] for 32 ONUs.

It can be observed in Fig. 4 that the power allocation per ONU reaches convergence for both schemes, i.e., DPCA-PID-FM and DPCA-PID-V. However, DPCA-PID-FM reaches convergence with a lower number of iterations than DPCA-PID-V. This behavior is directly related to DCPA-FM and DPCA-V, which represent the origins of DPCA-PID-FM and DPCA-PID-V. The addition of the proportional and differential procedures does not change the tendency of the DPCA-V delay in convergence compared with DPCA-FM.

Figure 5 shows the power allocation evolution per ONU for the number of iterations considering DPCA-PID-FM [Fig. 5(a)] and DPCA-PID-V [Fig. 5(b)] for 48 ONUs.

It can be observed in Fig. 5 that the power allocation per ONU reaches convergence for both schemes, i.e., DPCA-PID-FM and DPCA-PID-V. In addition, as illustrated previously, DPCA-PID-FM reaches full convergence with a lower number of iterations than DPCA-PID-V. Furthermore, the main result in Fig. 5 is the full convergence of DPCA-PID-FM in the same estimated weak-signal environment as DPCA-FM, illustrated in Fig. 3. Hence, the addition of the proportional and differential procedures changes the convergence behavior of DPCA-FM.

To elaborate further, a comparison between the velocity and the tendency of the convergence for the DPCAs previously discussed in this section is depicted in Fig. 6, the NMSE for 32 ONUs [Fig. 6(a)] and 48 ONUs [Fig. 6(b)].

It can be observed in Fig. 6(a) that the NMSEs for DPCA-FM and DPCA-PID-FM present the same performance in

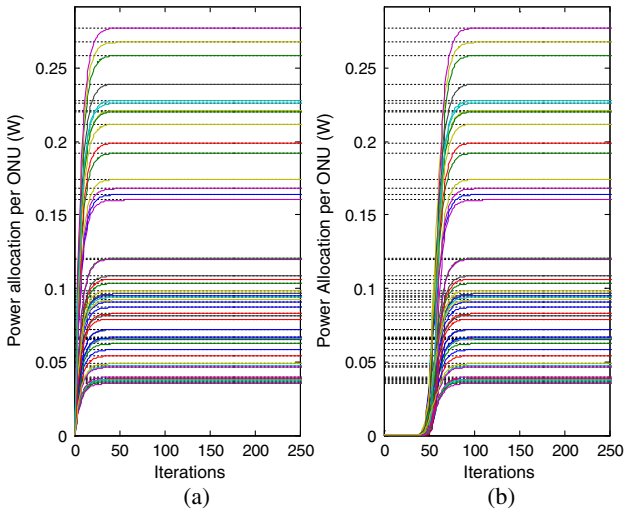

Fig. 5. PON-OCDMA with 32 ONUs. Power allocation per ONU for (a) DPCA-PID-FM and (b) DPCA-PID-V.

terms of rate of convergence for 32 ONUs, but with a marginal convergence gain (number of iterations for the same NMSE) for DPCA-PID-V related to DPCA-V. However, in Fig. 6(b) the NMSE for DPCA-FM is high and represents no convergence for a system with 48 ONUs. Also, for this number of ONUs DPCA-PID-FM achieves full convergence. In addition, it can be observed in Figs. 6(a) and 6(b) that the NMSE for DPCA-PID-V presents somewhat better convergence performance when compared with DPCA-V. The difference in the velocity of convergence between DPCA-PID-V and DPCA-V is just marginal at approximately 5 iterations. The addition of the proportional and differential procedures in DPCA-V does not change the rate of convergence.

Next, we analyze the channel estimation effect on the iterative DPCA convergence. Figure 7 depicts the NMSE evolution for the number of iterations for DPCA-FM and DPCA-V for 32 ONUs [Fig. 7(a)] and 48 ONUs [Fig. 7(b)]. In these results, the channel error estimation was considered to be $\delta = 0$, 0.1, 0.2, and 0.3. In addition, the NMSE evolution for the number of iterations considering DPCA-PID-FM and DPCA-PID-V is illustrated in Figs. 7(c) and 7(d) for 32 and 48 ONUs, respectively.

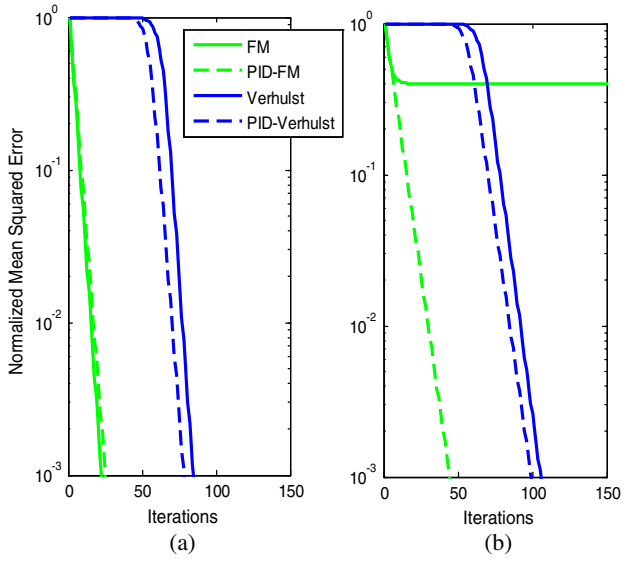

Fig. 6. NMSE for DPCA-FM, DPCA-V, DPCA-PID-FM, and DPCA-PID-V for (a) 32 ONUs and (b) 48 ONUs.

Figure 7 shows the impact of the channel error estimation on the performance of the DPCAs. Increasing the uncertainty causes convergence degradation of the allocation power per ONU, represented by the increasing NMSE. In addition, the channel error estimations have the same impact on both DPCA-PID-FM and DPCA-PID-V.

In order to evaluate the DPCA-PID-FM and DPCA-PID-V convergence performance and the quality of the solution under the time delay effects, Fig. 8 depicts the power allocation evolution per ONU for the number of iterations considering DPCA-PID-FM [Fig. 8(a)] and DPCA-PID-V [Fig. 8(b)] for 32 ONUs. In the remainder of this section, for the calculation of the total round-trip delays it was

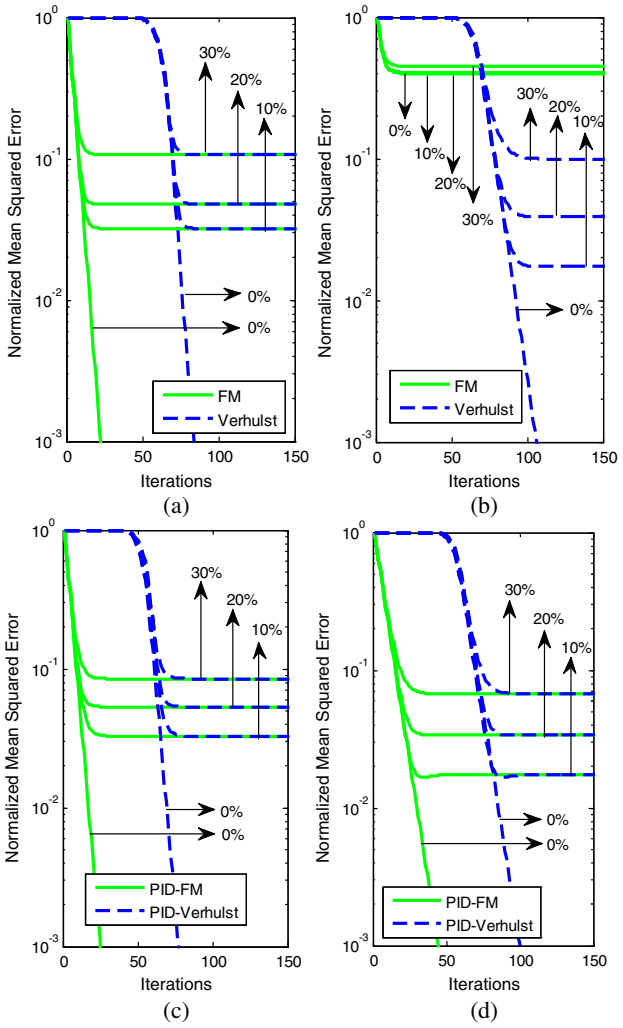

Fig. 7. NMSE for DPCA-FM and DPCA-V for (a) 32 and (b) 48 ONUs, and NMSE for DPCA-PID-FM and DPCA-PID-V for (c) 32 and (d) 48 ONUs. Channel error estimation of 0%, 10%, 20%, and 30%.

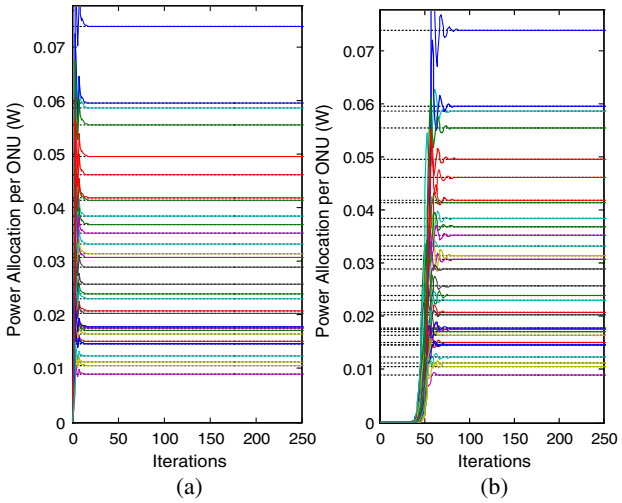

Fig. 8. PON-OCDMA with 32 ONUs. Power allocation per ONU for (a) DPCA-PID-FM and (b) DPCA-PID-V, considering the time delay effects.

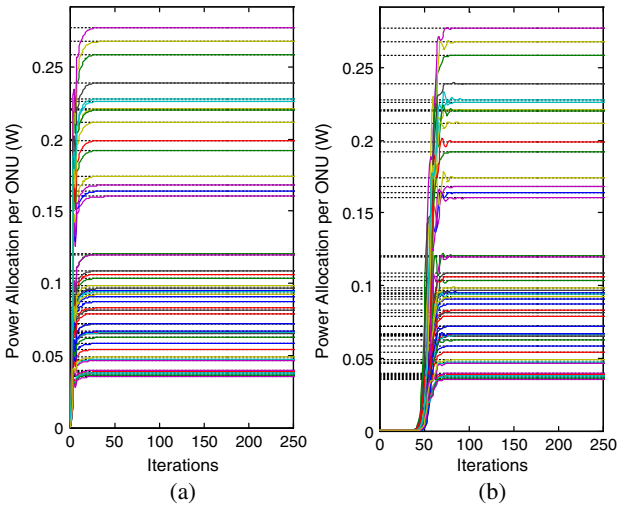

Fig. 9. PON-OCDMA with 48 ONUs. Power allocation per ONU for (a) DPCA-PID-FM and (b) DPCA-PID-V, considering the time delay effects.

considered that light propagates at approximately $\nu = 2 \times 10^5$ m/s in the fiber, and the power control algorithm is updated every 5 ms.

In Fig. 8 the impact of the time delay on the performance of DPCA-PID-FM and DPCA-PID-V can be observed. When the delay is considered, there is a variation in the transmitted power per user for initial iterations. In other words, the transmitted power per ONU converges toward the objective value while presenting oscillatory behavior. Furthermore, when Figs. 3 and 8 are compared, one can observe that when the delay effect is included, more iterations are necessary for the FM-DPCA algorithm to achieve full convergence for the same transmitted power.

In order to evaluate the DPCA-PID-FM and the DPCA-PID-V convergence performance and the quality of the solution under the time delay effects, Fig. 9 depicts the power allocation evolution per ONU for the number of iterations considering DPCA-PID-FM [Fig. 9(a)] and DPCA-PID-V [Fig. 9(b)] for 48 ONUs.

In Fig. 9 similar behavior can be observed to that presented in Fig. 8. However, there are some differences in the oscillatory behavior between Figs. 8 and 9 based on the amplitude of the transmitted power. To elaborate further, a comparison between the velocity and the tendency of the convergence for DPCA-PID-FM and DPCA-PID-FM previously discussed in this section is depicted in Fig. 10 for 32 ONUs [Fig. 10(a)] and 48 ONUs [Fig. 10(b)], considering the time delay effects.

It can be observed in Fig. 10(a) that the NMSEs for DPCA-PID-FM and DPCA-PID-V present almost the same performance in terms of rate of convergence for 32 ONUs; however, the oscillatory behavior introduced by the effect of the delay is related to the NMSE. In addition, in Fig. 10(b) the NMSEs for DPCA-PID-FM and DPCA-PID-FM for a system with 48 ONUs present similar tendencies, and the convergence is slightly accelerated compared with the system without delay.

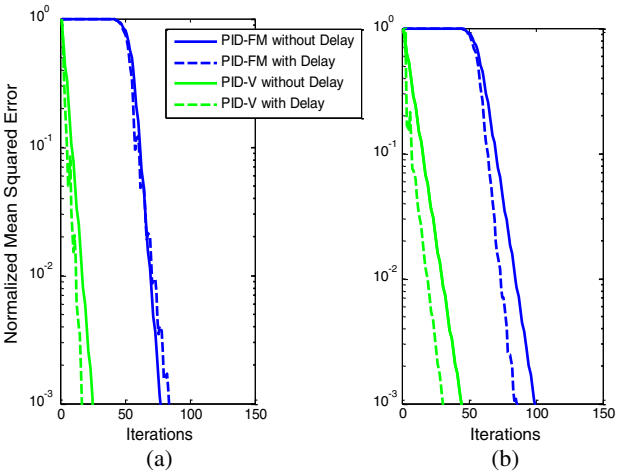

Fig. 10. NMSE for DPCA-FM, DPCA-V, DPCA-PID-FM, and DPCA-PID-V for (a) 32 ONUs and (b) 48 ONUs, considering time delay effects.

VI. Conclusion

The DPCAs based on the FM and Verhuslt models and PID algorithms have been investigated in this work for NG-PONs. The DPCAs of FM and Verhulst, which are represented by the classical control theory as an integral control, present a limitation in the accuracy of SNIR estimates when the network operates in weak-signal environments. Furthermore, the development of DPCA-PID-FM and DPCA-PID-V based on PID schemes originated by DPCA-FM and DPCA-V, respectively, has been conducted in this work to overcome the SNIR estimation limitation. The numerical results have demonstrated that DPCA-FM reaches full convergence with a lower number of iterations than DPCA-V for reliable SNIR estimates. Moreover, in estimated weak-signal scenarios, DPCA-V

has exhibited a smaller discrepancy from the optimum power vector solution and better convergence than DPCA-FM. In addition, adding the proportional and differential procedures in DPCA-V to originate DPCA-PID-V did not have an impact on the tendency and the rate of the convergence compared with DPCA-V. On the other hand, DPCA-PID-FM was able to change the partial convergence trend of DPCA-FM, substantially improving its performance. Finally, increasing the channel error estimation causes convergence error (or partial convergence) in all DPCAs studied in this work.

Acknowledgment

This work was supported in part by the National Council for Scientific and Technological Development (CNPq) of Brazil under grants 305522/2015-9, 202340/2011-2, and 304066/2015-0, and in part by CAPES and Londrina State University—Paraná State Government (UEL).

References

[1] H. Song, B. W. Kim, and B. Mukherjee, "Long-reach optical access networks: A survey of research challenges, demonstrations, and bandwidth assignment mechanisms," *IEEE Commun. Surv. Tutorials*, vol. 12, no. 1, pp. 112–123, 2010.

[2] E. Wong, "Next-generation broadband access networks and technologies," *J. Lightwave Technol.*, vol. 30, no. 4, pp. 597–608, 2012.

[3] M. de Andrade, M. Maier, M. P. McGarry, and M. Reisslein, "Passive optical network (PON) supported networking," *Opt. Switching Netw.*, vol. 14, pp. 1–10, 2014.

[4] S. Bindhaiq, A. Sahmah, M. Supaat, N. Zulkifli, A. B. Mohammad, R. Q. Shaddad, M. A. Elmagzoub, and A. Faisal, "Recent development on time and wavelength-division multiplexed passive optical network (TWDM-PON) for next-generation passive optical network stage 2 (NG-PON2)," *Opt. Switching Netw.*, vol. 15, pp. 53–66, 2015.

[5] T. Kodama, Y. Tanaka, S. Yoshima, N. Kataoka, J. Nakagawa, S. Shimizu, N. Wada, and K. Kitayama, "Scaling the system capacity and reach of a 10G-TDM-OCDM-PON system without an en/decoder at an ONU," *J. Opt. Commun. Netw.*, vol. 5, no. 2, pp. 134–143, 2013.

[6] S. Yoshima, Y. Tanaka, N. Kataoka, N. Wada, J. Nakagawa, and K. Kitayama, "Full-duplex, extended-reach 10G-TDM-OCDM-PON system without en/decoder at ONU," *J. Lightwave Technol.*, vol. 31, no. 1, pp. 43–49, 2013.

[7] D. A. Khotimsky, D. Zhang, L. Yuan, R. O. C. Hirafuji, and D. R. Campelo, "Unifying sleep and doze modes for energy-efficient PON systems," *IEEE Commun. Lett.*, vol. 18, no. 4, pp. 688–691, 2014.

[8] F. Durand and T. Abrão, "Energy-efficient power allocation for WDM/OCDM networks with particle swarm optimization," *J. Opt. Commun. Netw.*, vol. 5, no. 5, pp. 512–523, 2013.

[9] A. J. dos Santos, F. R. Durand, and T. Abrão, "Mitigation of environmental temperature variation effects in OCDMA networks using PSO power control," *J. Opt. Commun. Netw.*, vol. 7, no. 8, pp. 707–717, 2015.

[10] R. Matsumoto, T. Kodama, S. Shimizu, R. Nomura, K. Omichi, N. Wada, and K. I. Kitayama, "40G-OCDMA-PON system with an asymmetric structure using a single multi-port and sampled SSFBG encoder/decoders," *J. Lightwave Technol.*, vol. 32, no. 6, pp. 1132–1143, 2014.

[11] N. Tarhuni, T. Korhonen, M. Elmusrati, and E. Mutafungwa, "Power control of optical CDMA star networks," *Opt. Commun.*, vol. 259, pp. 655–664, 2006.

[12] L. Zulai, F. R. Durand, and T. Abrão, "Energy-efficient next-generation passive optical networks based on sleep mode and heuristic optimization," *Fiber Integr. Opt.*, vol. 34, no. 3, pp. 91–111, 2015.

[13] M. de Marques Paula, F. Durand, and T. Abrão, "WDM/OCDM energy-efficient networks based on heuristic ant colony optimization," *IEEE System J.*, to be published.

[14] Y. Pan and L. Pavel, "OSNR game optimization with link capacity constraints in general topology WDM networks," *Opt. Switching Netw.*, vol. 11, part A, pp. 1–15, 2014.

[15] G. Foschini and Z. Miljanic, "A simple distributed autonomous power control algorithm and its convergence," *IEEE Trans. Veh. Technol.*, vol. 42, no. 4, pp. 641–646, 1993.

[16] T. J. Gross, T. Abrão, and P. J. E. Jeszensky, "Distributed power control algorithm for multiple access systems based on Verhulst model," *Int. J. Electron. Commun.*, vol. 65, no. 4, pp. 361–372, 2011.

[17] F. R. Durand and T. Abrão, "Distributed SNIR optimization based on the Verhulst model in optical code path routed networks with physical constraints," *J. Opt. Commun. Netw.*, vol. 3, no. 9, pp. 683–691, 2011.

[18] D. U. Campos-Delgado, J. M. Luna-Rivera, and F. J. Martinez-Lopez, "Distributed power control algorithms in the uplink of wireless code-division multiple-access systems," *IET Control Theory Appl.*, vol. 4, no. 5, pp. 795–805, 2010.

[19] A. Paul, M. Akar, M. G. Safonov, and U. Mitra, "Adaptive power control for wireless networks using multiple controllers and switching," *IEEE Trans. Neural Netw.*, vol. 16, no. 5, pp. 1212–1218, 2005.

[20] A. M. Mayers, P. J. Benavidez, G. V. S. Raju, D. Akopian, and M. M. Jamshidi, "A closed-loop transmission power control system using a nonlinear approximation of power-time curve," *IEEE Syst. J.*, vol. 9, no. 3, pp. 1011–1019, 2015.

[21] G. Cincotti, N. Wada, and K. Kitayama, "Characterization of a full encoder/decoder in the AWG configuration for code-based photonic routers. Part I: Modelling and design," *J. Lightwave Technol.*, vol. 24, no. 1, pp. 103–112, 2006.

[22] G. Cincotti, "Design of optical full encoders/decoders for code-based photonic routers," *J. Lightwave Technol.*, vol. 22, no. 7, pp. 1642–1650, 2004.

[23] X. Wang, N. Wada, T. Miyazaki, G. Cincotti, and K.-I. Kitayama, "Field trial of 3-WDM × 10-OCDMA × 10.71-Gb/s asynchronous WDM/DPSK-OCDMA using hybrid E/D without FEC and optical thresholding," *J. Lightwave Technol.*, vol. 25, pp. 207–215, 2007.

[24] M. Ryosuke, K. Takahiro, M. Koji, W. Naoya, and K.-I. Kitayama, "Scalable two- and three-dimensional optical labels generated by 128-port encoder/decoder for optical packet switching," *Opt. Express*, vol. 23, no. 20, pp. 25747–25761, 2015.

[25] A. Lempel and H. Greenberger, "Families of sequences with optimal Hamming correlation properties," *IEEE Trans. Inform. Theory*, vol. 20, pp. 90–94, 1974.

[26] N. Stefanovic and L. Pavel, "An analysis of stability with time-delay of link level power control in optical networks," *Automatica*, vol. 45, no. 1, pp. 149–154, 2009.

[27] Y. Pan, T. Alpcan, and L. Pavel, "A system performance approach to OSNR optimization in optical networks," *IEEE Trans. Commun.*, vol. 58, no. 4, pp. 1193–1200, 2010.

[28] F. R. Durand, B. Angelico, and T. K. Abrão, "Analysis of delay and estimation uncertainty in power control model for optical CDMA network," *Opt. Switching Netw.*, vol. 21, pp. 67–78, 2016.

[29] P. Zhong, Y. Changyuan, and A. E. Willner, "Optical performance monitoring for the next generation optical communication networks," *Opt. Fiber Technol.*, vol. 16, pp. 20–45, 2010.

[30] C. Y. Yang and B. S. Chen, "Robust power control of CDMA cellular radio systems with time-varying delays," *Signal Process.*, vol. 90, no. 1, pp. 363–372, 2010.

[31] B. K. Lee, H. W. Chen, and B. S. Chen, "Power control of cellular radio systems via robust smith prediction filter," *IEEE Trans. Wireless Commun.*, vol. 3, no. 5, pp. 1822–1831, 2004.

[32] F. Gunnarsson and F. Gustafsson, "Control theory aspects of control in UMTS," *Control Eng. Practice*, vol. 11, no. 10, pp. 1113–1125, 2003.

[33] F. Gunnarsson and F. Gustafsson, "Dynamical effects of time delays and time compensation in power controlled DS-CDMA," *IEEE J. Sel. Areas Commun.*, vol. 19, no. 1, pp. 141–151, 2001.

[34] L. Sampaio, T. Abrão, B. Angelico, M. Lima, M. Proença, and P. Jeszensky, "Hybrid heuristic-waterfilling game theory approach in MC-CDMA resource allocation," *Appl. Soft Comput.*, vol. 12, pp. 1902–1912, 2011.

[35] K. H. Ang, G. Chong, and Y. Li, "PID control system analysis, design and technology," *IEEE Trans. Control Syst. Technol.*, vol. 13, no. 4, pp. 559–576, 2005.

Thiago A. Bruza Alves received a B.S. degree in electrical engineering from the North Paraná University in 2006. He is currently pursuing a master's degree in the Electrical Engineering Department of UEL—State University of Londrina (Brazil).

Fábio R. Durand received an M.S. degree in electrical engineering from the São Carlos Engineering School of São Paulo State, Brazil, in 2002 and a Ph.D. degree in electrical engineering from the State University of Campinas (UNICAMP), São Paulo, Brazil, in 2007. Now he is a Professor at the Technologic Federal University of Paraná (UTFPR) at Cornélio Procópio, Brazil. His research interests have been photonic technology, WDM/OCDM networks, heuristic and optimization aspects of OCDMA networks, and polarization mode dispersion impairments.

Bruno A. Angélico received a B.S. in electrical engineering from the State University of Londrina in 2003 and an M.Sc. in electrical engineering from Escola Politécnica of the University of São Paulo (EP-USP) in 2005. He was a Visiting Scholar at the California Institute for Telecommunications and Information Technology (Calit2), University of California, San Diego, in 2007–2008. He is currently an Assistant Professor at Escola Politécnica of the University of São Paulo (EP-USP), SP, Brazil. His research interests include ultra-wideband, multiple-input multiple-output (MIMO) systems, spread spectrum, and multi-user detection.

Taufik Abrão (SM'12, SM-SBrT) received B.S., M.Sc., and Ph.D. degrees in electrical engineering from the Polytechnic School of the University of São Paulo, São Paulo, Brazil, in 1992, 1996, and 2001, respectively. Since March 1997, he has been with the Communications Group, Department of Electrical Engineering, Londrina State University, Londrina, Brazil, where he is currently an Associate Professor of Communications Engineering. In 2012, he was an Academic Visitor with the Communications, Signal Processing and Control Research Group, University of Southampton, Southampton, UK. From 2007 to 2008, he was a Postdoctoral Researcher with the Department of Signal Theory and Communications, Polytechnic University of Catalonia (TSC/UPC), Barcelona, Spain. He has participated in several projects funded by government agencies and industrial companies. He is involved in the editorial board activities of six journals in the communication area, and he has served as TCP Member in several symposiums and conferences. He has served as an Editor for *IEEE Communications Surveys & Tutorials* since 2013, *IET Journal of Engineering* since 2014, and *IEEE Access* since 2016. He is a Senior Member of IEEE and SBrT-Brazil. His current research interests include communications and signal processing, especially multi-user detection and estimation, multicarrier code division multiple access and MIMO systems, cooperative communication and relaying, resource allocation, and heuristic and convex optimization aspects of 3G and 4G wireless systems. He has co-authored more than 200 research papers published in specialized/international journals and conferences.